Bulgarian Chemical Communications, Volume 51, Issue 4 (pp. 557 - 568) 2019 DOI: 10.34049/bcc.51.4.5055

Regression model and analysis of MHD mixed convective stagnation point nanofluid flow: SLM and SRM approach

B. Kumar[1*], G. S. Seth[1], R. Nandkeolyar[2]

[1]*Department of Applied Mathematics, Indian Institute of Technology (ISM), Dhanbad-826004, Jharkhand, India*
[2] *Department of Mathematics, National Institute of Technology, Jamshedpur - 831014, Jharkhand, India*

Received January 21, 2019; Revised April 4, 2019

The present paper is concerned with mixed convection, viscous and Joule dissipations, thermophoretic and Brownian diffusion effects on the steady stagnation point nanofluid flow with passive control of nanoparticles. Similarity transformation is exerted to convert governing boundary layer partial differential equations into ordinary differential equations without loss of generality. In order to optimize error and assess accuracy of solutions two different spectral schemes are efficiently employed to solve governing equations. The graphs for velocity, temperature and concentration of the present nanofluid flow model, obtained by using SLM (successive linearization method) and SRM (spectral relaxation method) are discussed in detail for various flow controlling parameters. Apart from it, regression analysis is performed for skin friction for making this model more effective in industries and engineering. Findings reflect that a boundary layer is formed even in case of the same stretching and free stream velocities in the presence of mixed convection parameter. Magnetic parameter is assisting parameter for the fluid flow when free stream velocity is dominant over stretching sheet velocity while in the opposite case it acts as opposing parameter for the velocity profile.

Keywords: Regression model, viscous and Joule dissipations, Brownian and thermophoretic diffusions, SLM (successive linearization method), SRM (spectral relaxation method)

INTRODUCTION

19th Century onwards, every country is running to thrive in all fields including technology and industries, for improving themselves and being the best. This race led to massive industrialization and many other activities. Therefore, we are getting beneficial outcomes, as well as direct consequences due to massive release of greenhouse gases. To mitigate the global warming, is a challenge for the world. This objective of reducing heat consumption can be achieved by increasing heat transfer. Therefore, nanofluids are introduced in the recent past, which are colloidal suspensions of nanosized particles in the base fluid. Masuda *et al*. [1] were the first to notice how heat transfer rate and thermal conductivity of liquid increases when ultra-fine particles are dispersed into it. They selected water as a base fluid and powders of Al_2O_3, TiO_2 and SiO_2 as ultrafine particles. Choi [2] coined the term nanofluid in his pioneering research. Some of the other relevant investigations are due to articles [3-5].

The models for fluid flow over a stretching/shrinking sheet are very important because of their large potential to deal with many industrial and engineering areas. They also have manifold applications in manufacturing of long and uniform metal parts, melt spinning technique for cooling liquid, metalworking process, etc. The pioneering attempt to observe a boundary layer flow over a continuous moving surface was done by Sakiadis [6]. Theoretically, a flow adjacent to a linearly stretching plate is studied by Crane [7]. Makinde and Aziz [8] efficiently employed the convective heated boundary condition to study nanofluid flow past a stretching sheet and found that as thermophoretic and Brownian diffusions become stronger; Sherwood number increases while Nusselt number decreases. Bhatti *et al*. [9] have taken a porous shrinking sheet to analyse the nonlinear thermal radiation effect on MHD nanofluid flow. Recently some other relevant research investigations are done by several authors [10-12], etc.

Natural convection is a process in which fluid motion is dependent on the density difference in the fluid, encountered as a result of temperature gradients. The force convection is a process in which fluid motion is developed by an external source like fan, pump, etc. When these two mechanisms occur simultaneously, then it is termed as mixed convection and is used in many thermal engineering processes. Various engineering and industrial processes such as transpiration cooling, aerodynamic extrusion, continuous filament extrusion, etc., can be qualitatively analysed by such types of models. Ghaly [13] has taken synchronized action of thermal radiation, buoyancy

* To whom all correspondence should be sent:
E-mail: chauhanbhuvan6@gmail.com

© 2019 Bulgarian Academy of Sciences, Union of Chemists in Bulgaria

force and magnetic field on the flow-field and suggested that local shear stress is decreasing function of radiation. MHD mixed convection flow with buoyancy effect is studied by Makinde *et al.* [14] taking viscous and Joule dissipations into account and reported that in case of a shrinking sheet dual solutions exist. They also found that skin friction decreases while local Nusselt number increases with enhancement in buoyancy force. Rashidi *et al.* [15] developed a very interesting model for forced convection flow of a nanofluid. Some more studies on this topic are due to articles [16-18].

Due to the wide use in engineering and industries, the flow near the stagnation point is investigated by many authors. The application of the flow behaviour near a fixed point is found in many problems such as manufacturing of plastic substance, metallurgy, lubricants theory, polymer extrusion, etc. Mustafa *et al.* [19] reported the boundary layer solutions of a stagnation point flow adjacent to a stretching sheet by homotopy analysis method. Rahman *et al.* [20] have taken inclined stretching cylinder and analysed the thermophysical aspect of stagnation point flow. Some other studies are due to articles [21, 22]

In the present investigation, our purpose is to present a boundary layer solution and observe the effect of various terms, *viz*. viscous and Joule dissipations, mixed convection, Brownian and thermophoretic diffusions on a stagnation point flow with passive control of nanoparticles by two different spectral schemes, i.e. SLM and SRM. As per authors concern, this model is not yet studied by a spectral scheme. There are several applications of such types of fluid flow models such as industrial cooling [23], nuclear reactor cooling [24], enhance the critical heat flux in pool boiling [25], reducing pollution and heating buildings [26], thermal energy storage [27], drug delivery [28], direct absorption solar collectors [29], friction reduction [30], etc.

MATHEMATICAL MODELLING OF THE PROBLEM

The present system deals with the steady two-dimensional, viscous, incompressible and electrically conducting stagnation point flow of a nanofluid over a stretching sheet with mixed convection, heat generation, viscous and Joule dissipations, Brownian and thermophoretic diffusions. The key assumptions which are made while deriving the governing equations are: the nanoparticles and base fluid are assumed in thermal equilibrium and chemical reaction between them is neglected; the nanofluid is viscous, incompressible and electrically conducting; the magnetic Reynolds number is small enough to discard the induced magnetic field; there is no external electric field so the induced electric field due to polarization of charges is negligible; and the Boussinesq approximation is taken into account, i. e. density variation obtained by concentration or temperature difference is neglected except in case of buoyancy force. The geometry of the concerned problem is presented in figure 1(a).

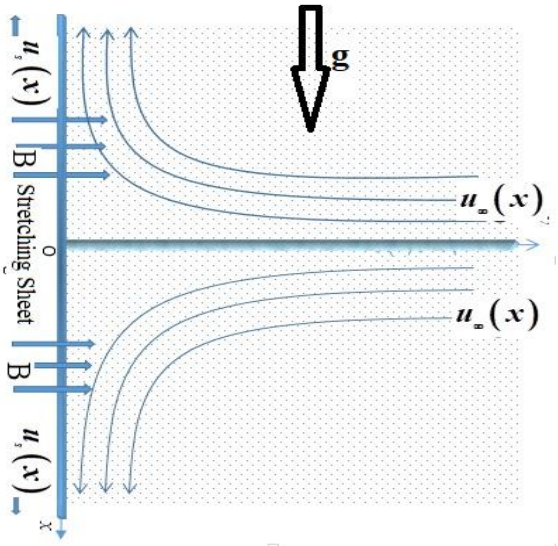

Fig 1(a). Schematic diagram and coordinate system of the flow problem.

The nanofluid is impinging normally over the stretching sheet and the stretching velocity is in the form of power law as $u_s = ax^n$. Free stream velocity of fluid is also taken in power law form as $u_\infty = bx^n$ where a, b and n are constants, i.e. fluid flow and stretching sheet are in upward direction along the x-axis. The symbols $T = T_s$ and $T = T_\infty$ are for constant temperature of fluid at the surface and in the free stream, respectively. The symbol C_∞ is for fluid concentration in the free stream while nanoparticle volume fraction C is controlled passively at the surface, as suggested by Kuznetsov and Nield [31]. For controlling boundary layer, transverse magnetic field having intensity B is exerted perpendicular to the sheet, i. e. along the y axis.

Using these key assumptions, the governing boundary layer equations, i.e. continuity, momentum, energy and concentration equations, are expressed, respectively, as follows:

$$\frac{\partial u}{\partial x}+\frac{\partial v}{\partial y}=0, \tag{1}$$

$$u\frac{\partial u}{\partial x}+v\frac{\partial u}{\partial y}=\upsilon\left(\frac{\partial^2 u}{\partial y^2}\right)+u_\infty\left(\frac{\partial u_\infty}{\partial x}\right)+\frac{\sigma}{\rho_{nf}}B^2\left(u_\infty-u\right)+\frac{g}{\rho_{nf}}\left(1-C_\infty\right)\rho_{nf\infty}\beta\left(T-T_\infty\right)-\frac{g}{\rho_{nf}}\left(C-C_\infty\right)\left(\rho_{np}-\rho_{nf\infty}\right) \tag{2}$$

$$\left(\rho c_p\right)_{nf}\left(u\frac{\partial T}{\partial x}+v\frac{\partial T}{\partial y}\right)=k\left(\frac{\partial^2 T}{\partial y^2}\right)+\sigma B^2\left(u_\infty-u\right)^2+\mu\left(\frac{\partial u}{\partial y}\right)^2+Q(T-T_\infty)+\left(\rho c_p\right)_{np}\left[D_B\left(\frac{\partial C}{\partial y}\frac{\partial T}{\partial y}\right)+\frac{D_T}{T_\infty}\left(\frac{\partial T}{\partial y}\right)^2\right], \tag{3}$$

$$u\frac{\partial C}{\partial x}+v\frac{\partial C}{\partial y}=\frac{D_T}{T_\infty}\left(\frac{\partial^2 T}{\partial y^2}\right)+D_B\left(\frac{\partial^2 C}{\partial y^2}\right). \tag{4}$$

Related boundary conditions are:

$$\left.\begin{aligned} &u=u_s, v=0, \frac{\partial C}{\partial y}=-\left(\frac{D_T}{D_B T_\infty}\right)\frac{\partial T}{\partial y},\\ &T=T_s, \text{ at } y=0,\\ &u\to u_\infty, C\to C_\infty, T\to T_\infty, \text{ as } y\to\infty, \end{aligned}\right\} \tag{5}$$

where meanings of symbols are given in the nomenclature section.

The similarity of flow states for two geometrically similar bodies for which the flow around the test body and the flow around prototype can be considered the same or similar if the Reynolds numbers in the two cases are equal [32, 33]. It will be true for other similarity parameters like Prandtl number, Schmidt number, etc. Due to this reason, we have considered it as a similar problem and similar solutions will be obtained. For similar solution of governing boundary layer equations (2), (3) and (4) along with boundary constraint (5), we have taken the following similarity transformations

$$\left.\begin{aligned} &\eta=y\sqrt{\frac{(n+1)u_s}{2\nu x}}, \psi=\sqrt{\frac{2u_s\nu x}{n+1}}f(\eta),\\ &\phi(\eta)=\frac{C-C_\infty}{C_\infty}, \theta(\eta)=\frac{T-T_\infty}{T_s-T_\infty}, \end{aligned}\right\} \tag{6}$$

where η is similarity variable and ψ is stream function while ϕ and θ are non-dimensional concentration and temperature, respectively.

Using these similarity variables, our problem was reduced to the following form:

$$f'''+ff''-\frac{2n}{n+1}f'^2-\frac{2M}{n+1}(f'-s)+\frac{2\lambda}{n+1}(\theta-Nr\phi)+\frac{2n}{n+1}s^2=0, \tag{7}$$

$$\frac{1}{Pr}\theta''+f\theta'+Nt\left(\theta'\right)^2+Nb\theta'\phi'+Ecf''^2+\alpha\theta+\frac{2MEc}{n+1}(f'-s)^2=0, \tag{8}$$

$$\phi''+Scf\phi'+\frac{Nt}{Nb}\theta''=0. \tag{9}$$

The boundary conditions (5) were reduced to the following form:

$$\left.\begin{aligned} &f(\eta)=0, f'(\eta)=1,\\ &Nb\phi'(\eta)+Nt\theta'(\eta)=0, \theta(\eta)=1, \text{ at } \eta=0,\\ &f'(\eta)\to s, \phi(\eta)\to 0, \theta(\eta)\to 0, \text{ as } \eta\to\infty, \end{aligned}\right\} \tag{10}$$

where:

$$M=\frac{\sigma B^2}{\rho_{nf}a}, \lambda=(1-C_\infty)\rho_{f_\infty}\frac{Gr_x}{Re_x^2},$$

$$Gr_x=\frac{g\beta\left(T_s-T_\infty\right)x^3}{\upsilon^2}, Re_x=\frac{u_s x}{\upsilon},$$

$$Nr=\frac{\left(\rho_p-\rho_{f_\infty}\right)C_\infty}{\rho_{f_\infty}\beta\left(1-C_\infty\right)\left(T_s-T_\infty\right)},$$

$$Nt=\frac{\left(\rho c_p\right)_{np}D_T\left(T_w-T_\infty\right)}{\left(\rho c_p\right)_{nf}T_\infty\upsilon}, Ec=\frac{u_s^2}{\left(c_p\right)_{nf}\left(T_s-T_\infty\right)},$$

$$Nb=\frac{\left(\rho c_p\right)_{np}D_B\left(C_\infty\right)}{\left(\rho c_p\right)_{nf}\upsilon}, \alpha=\frac{2Q_0}{(n+1)a(\rho c)_f},$$

$$Sc=PrLn=\frac{\upsilon}{D_B}, Pr=\frac{\upsilon}{\alpha}, Ln=\frac{\alpha}{D_B}, s=\frac{b}{a}.$$

For engineering purpose, it is important to find a dimensionless expression for skin friction Cf_x and local Nusselt number Nu_x which are defined respectively as:

$$Cf_x=\frac{\tau_s}{\rho u_s^2} \quad \text{and} \quad Nu_x=\frac{xq_s}{k(T_s-T_\infty)}. \tag{11}$$

Here τ_s is the shear stress at the surface and q_s heat flux at the surface which are defined by:

$$\tau_s=\mu\left(\frac{\partial u}{\partial y}\right)_{y=0} \text{ and } q_s=-k\left(\frac{\partial T}{\partial y}\right)_{y=0}. \tag{12}$$

Using similarity variable, we got the following dimensionless form of skin friction and local Nusselt number:

$$\left.\begin{aligned} &Cf_x Re_x^{1/2}=\sqrt{\frac{(n+1)}{2}}f''(0),\\ &Nu_x Re_x^{-1/2}=-\sqrt{\frac{(n+1)}{2}}\theta'(0). \end{aligned}\right\} \tag{13}$$

Here, θ'(0) is wall temperature gradient and f''(0) is wall velocity gradient.

SOLUTION METHODOLOGY

For finding solution of equations (7) to (9) along with boundary constraints (10) we have used two different spectral approaches, i. e. successive linearization method [34] and spectral relaxation method [35], to avoid inaccuracy of results.

Spectral methods take on a global approach to deal with the problem, i.e. the value of a derivative at a certain point in space depends on the solution at all the other points in space, and not just the neighbouring grid points. For this reason, spectral methods have excellent error properties with the so-called "exponential convergence" being the fastest possible, when the solution is smooth. Spectral methods are distinguished not only by the fundamental type of the method (Galerkin collocation, Galerkin with numerical integration), but also by the particular choice of the trial functions. Due to this fact, spectral methods usually have a very high order of approximation. In fact, spectral methods were among the first to be used in practical flow simulations. Because of their simplicity, rapid convergence and high accuracy, we conclude that the SLM and SRM have great potential of being used in place of the traditional methods such as finite difference method, shooting technique along with Runge Kutta method, finite element method, etc., in solving nonlinear boundary value problems.

SUCCESSIVE LINEARIZATION METHOD (SLM)

For applying this technique, the functions f(η), θ(η), and ϕ(η) can be assumed as:

$$\left.\begin{aligned} f(\eta) &= f_j(\eta) + \sum_{w=0}^{j-1} F_w(\eta), \\ \theta(\eta) &= \theta_j(\eta) + \sum_{w=0}^{j-1} \Theta_w(\eta), \\ \phi(\eta) &= \phi_j(\eta) + \sum_{w=0}^{j-1} \Phi_w(\eta), \end{aligned}\right\} \tag{14}$$

where functions f(η), θ(η), and ϕ(η) are unknown and $F_w(\eta)$, $\Theta_w(\eta)$, and $\Phi_w(\eta)$, are successive approximations. The next algorithm to use SLM is to choose initial guess, i.e:

$$\left.\begin{aligned} F_0(\eta) &= 1 - s + s\eta - (1-s)e^{-\eta}, \\ \Theta_0(\eta) &= e^{-\eta},\ \Phi_0(\eta) = -\frac{Nt}{Nb}e^{-\eta}. \end{aligned}\right\} \tag{15}$$

Here F_0, Θ_w and Φ_0 are the initial guesses that satisfy boundary conditions for f, θ and ϕ. The solutions of f(η), θ(η), and ϕ(η), after M iterations can be expressed as:

$$\left.\begin{aligned} f(\eta) &\approx \sum_{w=0}^{M} F_w(\eta), \theta(\eta) \approx \sum_{w=0}^{M} \Theta_w(\eta), \\ \phi(\eta) &\approx \sum_{w=0}^{M} \Phi_w(\eta). \end{aligned}\right\} \tag{16}$$

The Chebyshev spectral collocation scheme is utilized to obtain a solution of these linearised equations. This scheme uses those polynomials which are defined on [-1, 1] closed interval. So, for using this method we have to convert the domain $[0, \infty)$ to [-1, 1] with the help of the domain truncation methodology. In this method, the solution of the problem is obtained in the interval $[0, L^*]$ in place of $[0, \infty)$ by utilising the following transformation:

$$\frac{\eta}{L^*} = \frac{\zeta + 1}{2}, -1 \le \zeta \le 1. \tag{17}$$

Here L^* is the scaling parameter. This parameter is very significant due to its use in implementing boundary conditions at infinity. Let P be the number of collocation points and Gauss-Lobatto collocation points method is used to discretize the domain [-1, 1] which is defined as follows:

$$\zeta = \cos\frac{\pi i}{P}, i=0,1,2.....P. \tag{18}$$

At these P collocation points the functions F_j, Θ_j and Φ_j for $j \ge 1$ are approximated with the help of kth Chebyshev polynomial (T_k^*) as:

$$\left.\begin{aligned} F_j(\zeta) &\approx \sum_{k=0}^{P} F_j(\zeta_k) T_k^*(\zeta_k), \\ \Theta_j(\zeta) &\approx \sum_{k=0}^{P} \Theta_j(\zeta_k) T_k^*(\zeta_k), \\ \Phi_j(\zeta) &\approx \sum_{k=0}^{P} \Phi_j(\zeta_k) T_k^*(\zeta_k), \end{aligned}\right\} \tag{19}$$

Kth Chebyshev polynomial is defined as:

$$T_k^*(\zeta) = \cos[k \cos^{-1}(\zeta)]. \tag{20}$$

At the collocation points, the r^{th} derivatives of functions F_j, Θ_j and Φ_j are constructed as:

$$\left.\begin{aligned} \frac{d^r F_j}{d\eta^r} &= \sum_{k=0}^{P} S_{ki}^r F_j(\zeta_k), \\ \frac{d^r \Theta_j}{d\eta^r} &= \sum_{k=0}^{P} S_{ki}^r \Theta_j(\zeta_k), \\ \frac{d^r \Phi_j}{d\eta^r} &= \sum_{k=0}^{P} S_{ki}^r \Phi_j(\zeta_k). \end{aligned}\right\} \tag{21}$$

Here $S = 2D / L^*$ where D is a matrix called Chebyshev differentiation matrix and the entries of this matrix are as follows:

$$\left.\begin{aligned} D_{00} &= \frac{2P^2+1}{6},\ D_{ik} = \frac{c_i(-1)^{i+k}}{c_k\zeta_i - \zeta_k}, \\ & \qquad i \neq k; k=0,..P, \\ D_{PP} &= -\frac{2P^2+1}{6}, D_{kk} = -\frac{\zeta_k}{2(1-\zeta_k^2)}, \\ & \qquad k=1,.....P-1. \end{aligned}\right\} \quad (22)$$

In this procedure, we get the following matrix equation:

$$A_{j-1}X_j = R_{j-1}, \quad (23)$$

where A_{j-1} is a (3P+3)×(3P+3). square matrix. X_j and R_{j-1} are $(3P+3)\times 1$ column vectors defined by:

$$A_{j-1} = \begin{bmatrix} A_{11} & A_{12} & A_{13} \\ A_{21} & A_{22} & A_{23} \\ A_{31} & A_{32} & A_{33} \end{bmatrix}, \quad x_j = \begin{bmatrix} F_j \\ \Theta_j \\ \Phi_j \end{bmatrix}, \ R_{j-1} = \begin{bmatrix} r_{1,j-1} \\ r_{2,j-1} \\ r_{3,j-1} \end{bmatrix}, \quad (24)$$

where:

$$F_j = [f_j(\zeta_0), f_j(\zeta_1), ...f_j(\zeta_{P-1}), f_j(\zeta_P)]^T,$$
$$\Theta_j = [\theta_j(\zeta_0), \theta_j(\zeta_1), ...\theta_j(\zeta_{P-1}), \theta_j(\zeta_P)]^T,$$
$$\Phi_j = [\phi_j(\zeta_0), \phi_j(\zeta_1), ...\phi_j(\zeta_{P-1}), \phi_j(\zeta_P)]^T,$$
$$r_{1,j-1} = [r_{1,j-1}(\zeta_0), r_{1,j-1}(\zeta_1), ..., r_{1,j-1}(\zeta_P)]^T,$$
$$r_{2,j-1} = [r_{2,j-1}(\zeta_0), r_{2,j-1}(\zeta_1), ..., r_{2,j-1}(\zeta_P)]^T,$$
$$r_{3,j-1} = [r_{3,j-1}(\zeta_0), r_{3,j-1}(\zeta_1), ..., r_{3,j-1}(\zeta_P)]^T,$$
$$A_{1,1} = a_{1,j-1}D^3 + a_{2,j-1}D^2 + a_{3,j-1}D + a_{4,j-1}I,$$
$$A_{1,2} = a_{5,j-1}I,\ A_{1,3} = a_{6,j-1}I,$$
$$A_{2,1} = b_{1,j-1}D^2 + b_{2,j-1}D + b_{3,j-1}I,$$
$$A_{2,2} = b_{4,j-1}I + b_{5,j-1}D + b_{6,j-1}D^2,$$
$$A_{2,3} = b_{7,j-1}I,\ A_{3,1} = c_{1,j-1}D^2 + c_{2,j-1}D + c_{3,j-1}I,$$
$$A_{3,1} = c_{1,j-1}D^2 + c_{2,j-1}D + c_{3,j-1}I,$$
$$A_{3,2} = c_{4,j-1}D^2 + c_{5,j-1}D + c_{6,j-1}I,\ A_{3,3} = c_{7,j-1}D.$$

In these equations, T shows transpose and $a_{k,j-1}$, $b_{k,j-1}$, $c_{k,j-1}$, $d_{k,j-1}$ are diagonal matrices. I and O are identity matrix and zero matrix, respectively, of order (P+1)×(P+1). Ultimately, the solution is given by:

$$X_j = A_{j-1}^{-1}R_{j-1}. \quad (25)$$

OVERVIEW OF SPECTRAL RELAXATION METHOD (SRM)

The brief explanation of SRM to solve the system of equations (7) to (9) with boundary conditions (10) is provided in this section. Gauss Seidel approach is utilized in this method to linearize and decouple a system of differential equations. We have denoted the current iteration label by (r+1) and the previous iteration which is assumed to be known is denoted by r. For applying SRM algorithm, we have assumed the following:

$$f'_{r+1} = p_r,\ f_{r+1}(0) = 0 \quad (26)$$

The linearised and decoupled form of equations (7) to (9) with boundary conditions (10) is given by:

$$p_{r+1}'' + f_{r+1}p_{r+1}' - \frac{2M}{n+1}p_{r+1} = \frac{2n}{n+1}p_r^2 - \frac{2Ms}{n+1} - \frac{2\lambda}{n+1}(\theta_{r+1} - Nr\phi_{r+1}) - \frac{2n}{n+1}s^2 \quad (27)$$

$$\frac{1}{Pr}\theta_{r+1}'' + f_{r+1}\theta_{r+1}' + \alpha\theta_{r+1} = -Nt(\theta_r')^2 - Nb\theta_r'\phi_r' - Ec(p_{r+1}')^2 - \frac{2MEc}{n+1}(p_{r+1}-s)^2 \quad (28)$$

$$\phi_{r+1}'' + Scf_{r+1}\phi_{r+1}' = -\frac{Nt}{Nb}\theta_{r+1}'' \quad (29)$$

with the boundary conditions:

$$\left.\begin{aligned} p_{r+1}(\eta) &= 1,\ Nb\phi_{r+1}'(\eta) + Nt\theta_{r+1}'(\eta) = 0, \\ & \qquad \theta_{r+1}(\eta) = 1, \ \text{at}\ \eta = 0, \\ p_{r+1}(\eta) &\to s,\ \phi_{r+1}(\eta) \to 0, \\ & \qquad \theta_{r+1}(\eta) \to 0, \ \text{as}\ \eta \to \infty. \end{aligned}\right\} \quad (30)$$

To solve these decoupled equations, Chebyshev spectral collocation technique was used in which domain is transformed from the interval [0 L^*] to [-1 1], with suitable transformation where L^* is scaling parameter. Equations (26) to (29) can be transformed as follows:

$$A_1f_{r+1} = B_1,\ A_2p_{r+1} = B_2,$$
$$A_3\theta_{r+1} = B_3,\ A_4\phi_{r+1} = B_4,$$

where

$$A_1 = D^1,\ B_1 = p_r,$$
$$A_2 = D^2 + \text{diag}(f_{r+1})D - \text{diag}\left(\frac{2M}{n+1}\right)I,$$
$$B_2 = \frac{2n}{n+1}p_r^2 - \frac{2Ms}{n+1} - \frac{2\lambda}{n+1}(\theta_{r+1} - Nr\phi_{r+1}) - \frac{2ns^2}{n+1},$$

$$A_3 = \mathrm{diag}(1/\mathrm{Pr})D^2 + \mathrm{diag}(f_{r+1})D + \mathrm{diag}(\alpha)I,$$

$$B_3 = -Nt(\theta_r')^2 - Nb\theta_r'\phi_r' - Ec(p_{r+1}')^2 - \frac{2MEc}{n+1}(p_{r+1} - s)^2,$$

$$A_4 = D^2 + \mathrm{diag}(Scf_{r+1})D,\ B_4 = -\frac{Nt}{Nb}\theta_{r+1}''.$$

Here Diag() and I are diagonal and identity matrices, respectively, of order (P+1)×(P+1), where P is the number of grid points. The initial guess that is chosen to solve equations (26) to (29) that satisfies boundary condition (30) is given by:

$$f_0 = 1 - s + s\eta - (1-s)e^{-\eta}, p_0 = s + (1-s)e^{-\eta},$$

$$\theta_0(\eta) = e^{-\eta},\ \phi_0(\eta) = -\frac{Nt}{Nb}e^{-\eta}.$$

SOLUTION ERROR (SRM)

The solution error method is used to check the convergence of the solutions. In this method, the norm of the difference of the solution at various iterations is calculated and if this value tends to very small then the method converges. The errors [36] in the solution of $f(\eta)$, $\theta(\eta)$, and $\phi(\eta)$ are given as:

$$\mathrm{errorF} = P\left\| f_{r+1}^{n+1} - f_r^{n+1} \right\|_\infty,$$

$$\mathrm{errorT} = P\left\| \theta_{r+1}^{n+1} - \theta_r^{n+1} \right\|_\infty,$$

$$\mathrm{errorG} = P\left\| \phi_{r+1}^{n+1} - \phi_r^{n+1} \right\|_\infty.$$

The errors in the solutions are portrayed in Figs. 1(b)-1(d). After fifty iterations we got the minimum error.

VALIDATION OF APPROXIMATE SOLUTION

To validate our results, we have compared skin friction and local Nusselt number for different input parameters *via* two different approaches, SLM and SRM which are presented in Tables 1 and 2.

There is an excellent agreement between the results obtained by these schemes. In addition to it, a comparison of local Nusselt number between our results and those of Ishfaq *et al*. [37] was performed by nullifying extra parameters (see table 3). Excellent agreement between them leads to approvement of the present solutions.

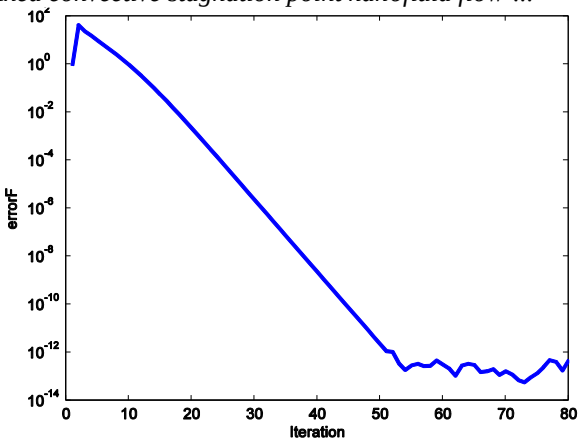

Fig 1(b). Solution error for $f(\eta)$

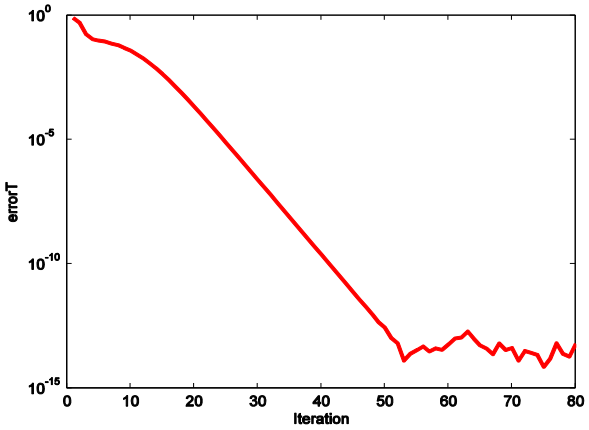

Fig 1(c). Solution error for $\phi(\eta)$

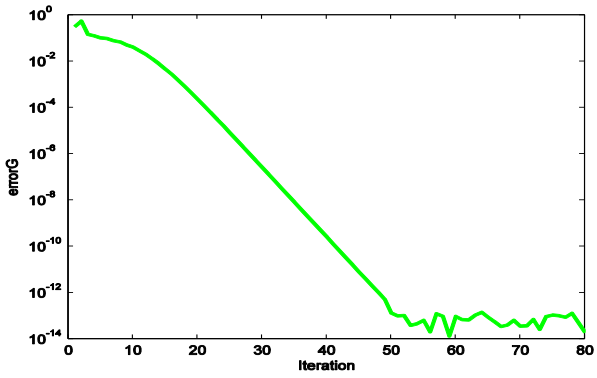

Fig 1(d). Solution error for $\theta(\eta)$.

Table 1. Values of skin friction and local Nusselt number for different flow parameters by SLM

M	λ	Sc	Nt	Nb	s	$Cf_x Re_x^{1/2}$ (SLM)	$Nu_x Re_x^{-1/2}$ (SLM)	CPU Time (Sec)
1						1.15150341	-1.37468956	3.247
3						0.88942638	-1.27033132	5.965
5						0.65057101	-1.18196765	8.742
	0					-1.12725825	-1.09985601	3.321
	5					-0.02590419	-1.2873988	6.231
	10					1.01728621	-1.32014235	8.796
		1				1.02180356	-1.40933744	2.987
		2				1.01355207	-1.36085112	5.654
		4				1.02375922	-1.2854098	8.215
			0.1			0.9111903	-1.41121177	3.984
			0.2			1.01728621	-1.32014235	6.742
			0.3			1.12567155	-1.22570304	9.281
				0.1		1.12872826	-1.29920906	2.946
				0.2		1.01728621	-1.32014235	5.852
				0.3		0.97949569	-1.32637838	8.742
					0.5	1.01728621	-1.32014235	4.511
					1	2.13083584	-1.50721597	6.423
					1.5	3.71647164	-1.2249959	9.836

Table 2. Values of skin friction and local Nusselt number for different flow parameters by SRM

M	λ	Sc	Nt	Nb	s	$Cf_x Re_x^{1/2}$ (SRM)	$Nu_x Re_x^{-1/2}$ (SRM)	CPU Time (Sec)
1						1.151512	-1.37463	4.852
3						0.889423	-1.27035	7.499
5						0.650573	-1.18198	10.842
	0					-1.127248	-1.09981	3.427
	5					-0.025904	-1.2873	6.732
	10					1.017285	-1.32017	9.537
		1				1.021802	-1.40931	5.632
		2				1.013553	-1.36082	8.432
		4				1.0237129	-1.2854	11.211
			0.1			0.91119	-1.41121	3.673
			0.2			1.017285	-1.32017	5.763
			0.3			1.125673	-1.22570	7.834
				0.1		1.128729	-1.29924	3.984
				0.2		1.017285	-1.32017	5.975
				0.3		0.979474	-1.32632	9.392
					0.5	1.017285	-1.32017	4.521
					1	2.130834	-1.50724	8.291
					1.5	3.716474	-1.2249	11.211

Table 3. Comparison of local Nusselt number $Nu_x Re_x^{-1/2}$ with Ishfaq *et al.* [37] when Nb = 0.1 and Sc = 10

Nt	Pr = 14.2		Pr = 21	
	Present result (SLM)	Ishfaq *et al.* [37]	Present result (SLM)	Ishfaq *et al.* [37]
0.1	2.48347	2.4835	3.02857	3.0286
0.2	2.18151	2.1815	2.61673	2.6167
0.3	1.89587	1.8959	2.22533	2.2253
0.4	1.63714	1.6371	1.87618	1.8762
0.5	1.41258	1.4126	1.58418	1.5842

RESULTS AND DISCUSSION

The numerical computation of the present model is performed in this article by using two different schemes, i.e. SRM and SLM, for selected flow controlling parameters such as M, Nb, Ec, etc. For the current study default values of input parameters for numerical simulation are taken as M = 2, n = 1, λ = 10, Nr = 0.2, s = 0.5, Pr = 6.2, Nb = 0.2, Nt = 0.2, Ec = 0.1, Sc = 3, and α = 0.2 until otherwise stated. In table 1 it is clearly depicted that parameters λ, Nt, s have a tendency to enhance skin friction at the surface while parameters M and Nb have the reverse effect on it. The parameters M, Sc and Nt show a decreasing nature for local

Nusselt number but λ and Nb have tendency to enhance the rate of heat transfer in magnitude.

The distribution of velocity with various flow controlling parameters is displayed in figures 1(e) to 1(h).

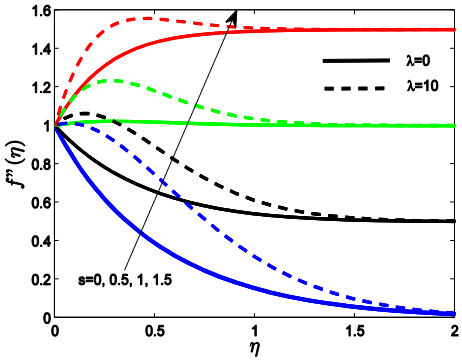

Fig1(e). Velocity profiles for different values of s

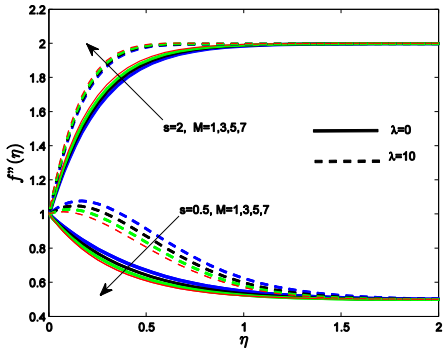

Fig 1(f). Velocity profiles for different values of M

The velocity distribution for disparate values of the stagnation parameter along with the mixed convection parameter is portrayed in Fig. 1(e). It is suggested here that when a free stream is moving faster than the stretching velocity, i. e. $s > 1$, the increment in s increases velocity distribution and the same effect is observed in $s < 1$ case. It is the main observing point here that in absence of a mixed convection parameter there is no boundary layer when stretching and free stream velocity are the same but in presence of mixed convection a boundary layer is observed to form and more precisely, the momentum boundary layer thickness tends to decrease as increment in s.

This phenomenon is the sole contribution of buoyancy forces acting on the flow-field. The nature of velocity for different values of M and two different values of s and λ is revealed in Fig. 1(f).

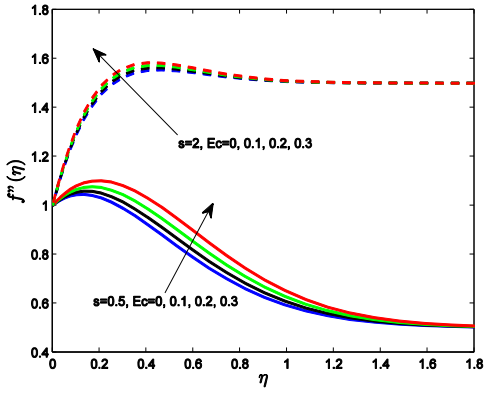

Fig 1(g). Velocity profiles for different values of Ec

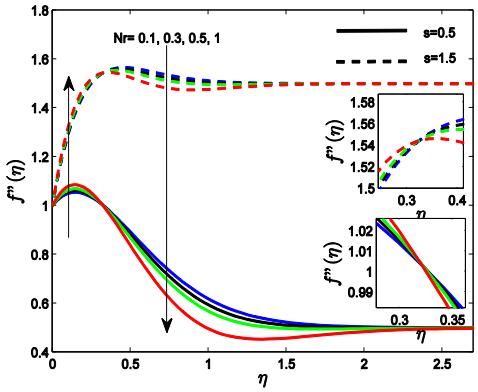

Fig 1(h). Velocity profiles for different values of Nr

It is widely accepted that M has a tendency to slow down the velocity because Lorentz force behaves as a resistive force that retards the motion. But in the present situation there is a dual nature of velocity for two different values of s. When $s > 1$, M acts as assisting parameter for flow while for $s < 1$, M has a tendency to decrease the velocity. This event is due to the fact that when $s > 1$ free stream velocity is dominant over stretching velocity. Tendency of M for $s > 1$ is also reported in [38, 39]. Fig. 1(g) displays the velocity distribution for various values of Eckert number. It is concluded from the figure that increment in parameter Ec boosts the velocity and increases boundary layer thickness due to an increment in kinetic energy. The velocity behaviour for parameter Nr is depicted in Fig. 1(h) which indicates a dual behaviour of buoyancy ratio parameter on fluid velocity, i. e. near the sheet velocity distribution increases and as going away form sheet, it acts as opposing parameter for the flow.

Figures 2(a) to 2(d) display the temperature distribution for various pertaining parameters.

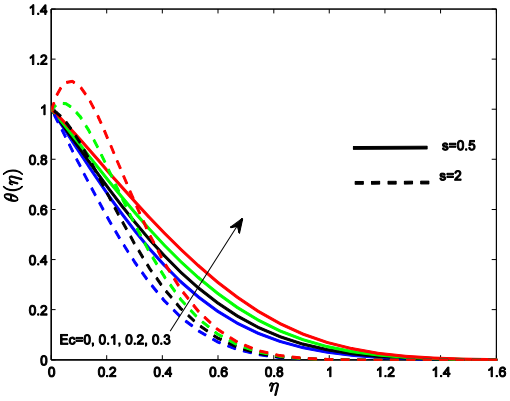

Fig 2(a). Temperature profiles for different values of Ec.

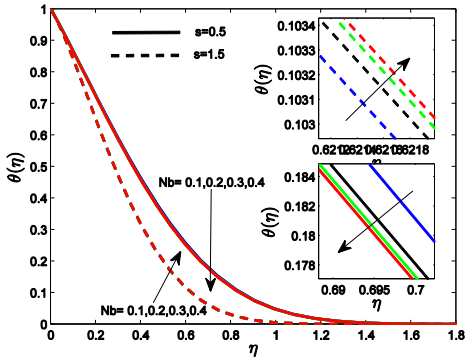

Fig 2(b). Temperature profiles for different values of Nb.

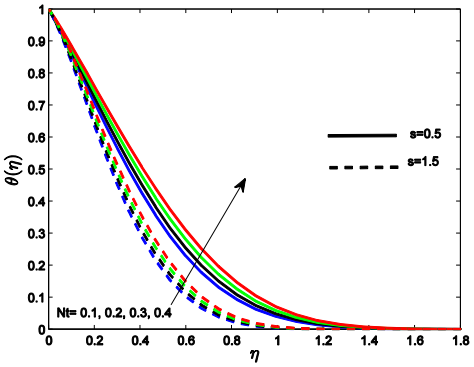

Fig 2(c). Temperature profiles for different values of Nt**.**

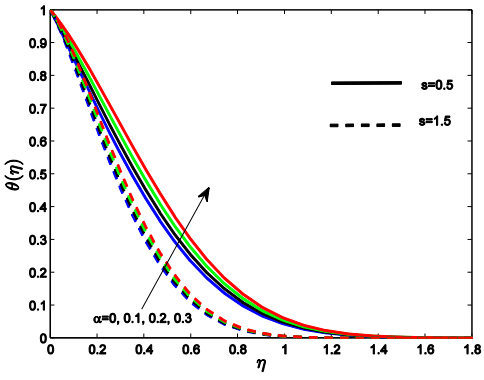

Fig 2(d). Temperature profiles for different values of α.

It is interesting to note from Figs. 2(a)-2(d) that the thermal boundary layer is thinner in case of $s>1$ than that of s<1. Fig. 2(a) illustrates the temperature profiles for various values of Ec. It can be seen here that when s<1 or s>1, increasing behaviour of temperature profile is found with an increase in Eckert number. When s>1 a hump is found in the region near the sheet on increasing Ec, also fluid temperature approaches free stream value quicker for s>1. This influence of Ec on the temperature profile is encountered due to the increasing nature of viscous and Joule dissipations. The tendency of viscous and Joule heating is to generate heat, which is due to friction between two adjacent electrically conducting fluid layers thereby increasing fluid temperature. Temperature distribution for different values of Brownian motion parameter is displayed in Fig. 2(b) which depicts the opposite nature of temperature towards Brownian motion parameter for $s<1$, but for $s>1$ Nb acts as assisting parameter for the temperature profile. Same behaviour of Nb for $s<1$ is also found by Halim *et al*. [40]. The behaviour of temperature distribution towards parameter Nt can be seen in Fig. 2(c). The fact which is visualized here is that parameter Nt acts as assisting parameter for temperature distribution and significant increment is found in thermal boundary layer width. Increment in Nt means increase in thermophoretic phenomenon which is the particle analogous phenomenon. Therefore, nanoparticles transport thermal energy with increment in Nt due to collision of particles from hot surface into boundary layer, so increment in temperature is found. Fig. 2(d) displays the heat generation effect on the temperature profile which indicates that increment in temperature is found on increasing heat generation parameter. It is quite obvious that the heat source emits heat in the flow region, therefore, fluid temperature rises.

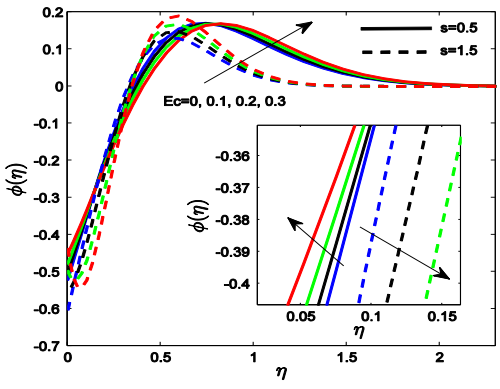

Fig 2(e). Concentration profiles for different values of Ec.

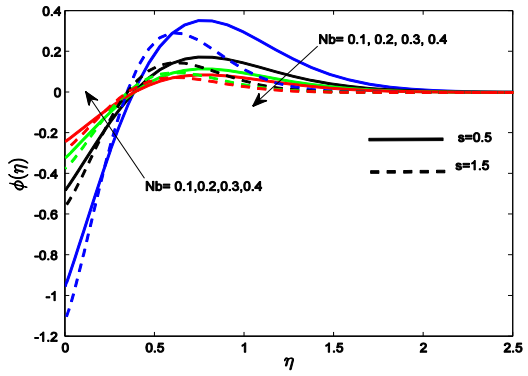

Fig 2(f). Concentration profiles for different values of Nb.

The concentration distribution for various values of input parameters is shown in Figs. 2(e) to 2(g). These profiles start with a negative value and after obtaining a positive peak they start approaching towards free stream. The numerical values of concentration are negative in the region close to the stretching sheet. This may be due to passive control of species concentration and it is dominant in the region close to sheet than that in the region away from the sheet within the concentration boundary layer.

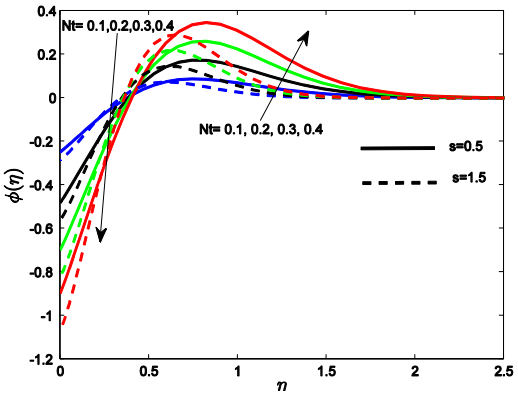

Fig 2(g). Concentration profiles for different values of Nt

Table 4. Error bound and quadratic regression coefficients for the estimated $Cf_x Re_x^{1/2}$

s	n	Cf	e_1	e_2	e_3	e_4	e_5	m_f
0.5	1	-0.89501	-0.24844	0.44092	0.02051	-0.00262	-0.01327	2.55E-05
	2	-0.91406	-0.11542	0.22577	0.00418	-0.00107	-0.00375	5.21E-06
1.5	1	1.75346	0.14461	0.37040	-0.00036	0.00013	-0.0146	5.87E-04
	2	1.74464	0.073601	0.19009	-0.00098	-0.00031	-0.00387	2.60E-04

Fig. 2(e) presents the effect of parameter Ec on concentration distribution and it is visualised here that, when $s<1$ initial concentration decreases in magnitude and when $s>1$ initial increment in concentration is found but in both cases concentration profiles obtain a positive peak and finally tend to increase as approaching the free stream. This event is the contribution of increment in kinetic energy and reduction of nanoparticle migration as increment in Ec. Fig. 2(f) portrays the influence of Nb which indicates that enhancement in Nb tends to dilute concentration throughout the boundary layer because increment in Nb leads to increase the diffusion of nanoparticles inside the boundary layer. However, opposite impact of Nt can be seen from Fig. 2(g) because increment in Nt increases thermophoretic phenomena, which leads to weaken the transport of nanoparticles near the sheet. These two figures also suggest that when s<1, this phenomenon is stronger than that when s>1.

A QUADRATIC MULTIPLE REGRESSION MODEL

In this section estimation of skin friction is performed with the help of quadratic regression model. For performing it on skin friction we have generated values of M and λ randomly from the set of 100 values that are taken from the interval [0.5 2] and [0 10], respectively, while values of other parameters are taken fixed. The approximated quadratic regression model for $Cf_x\sqrt{Re_x}$ is given as follows:

$$Cf_{est} = Cf + e_1 M + e_2 \lambda + e_3 M^2 + e_4 \lambda^2 + e_5 M\lambda, \quad (31)$$

Following formula is used to find the maximum relative error:

$$\varepsilon_1 = \left|Cf_{est} - Cf\right| / \left|Cf\right|. \quad (32)$$

Table 4 presents the regression coefficients of this estimation along with the maximum relative error. It is visible from table 4 that whether free stream velocity is dominant over the stretching sheet or conversely, the regression coefficient of λ is greater than the regression coefficient of M which reflects that small variation in λ leads to larger perturbation in skin friction in comparison to M. It is also interesting to note that when n increases, the regression coefficients of both M and λ decrease in magnitude.

CONCLUSION

Throughout the present mathematical model of stagnation point nanofluid flow over stretching sheet, our main focus is to find flow controlling parameters effect on fluid velocity, concentration,

temperature along with skin friction and heat flux. The parameters s and Ec have tendency to enhance fluid velocity. Apart from it when s<1 the magnetic parameter shows the obvious result, i.e. decrement in velocity distribution but when s>1 the magnetic parameter acts as assisting parameter for fluid velocity. The parameter Nr enhances the velocity near the sheet but while approaching free stream it tends to decrease. Temperature distribution is enhanced due to increment in parameters Ec, Nt and α. The parameter Nb acts as assisting parameter for temperature for s>1 while for s<1, it acts as opposing parameter. Parameter Nb leads to dilute concentration throughout the boundary layer while thermophoretic parameter increases it.

REFERENCES

1. H. Masuda, A. Ebata, K. Teramae, *Netsu Bussei*, **7**, 227 (1993).
2. S. U. S. Choi, *ASME-Publications-Fed.*, **231**, 99 (1995).
3. M. M. Rashidi, M. M. Bhatti, M. A. Abbas, M. E. Ali, *Entropy*, **18**, 117 (2016).
4. M. A. Abbas, Y. Bai, M. M. Rashidi, M. M. Bhatti, *Entropy* , **18**, 90 (2016).
5. T. Abbas, M. Ayub, M. M. Bhatti, M. M. Rashidi, M. E. Ali, *Entropy*, **18**, 223 (2016).
6. B. C. Sakiadis, *AIChE J.*, **7**, 26 (1961).
7. L. J. Crane, *Z. Angew. Math. Phys.*, **21**, 645 (1970).
8. O. D. Makinde, A. Aziz, *Int. J. Therm. Sci.*, **50**, 1326 (2011).
9. M. M. Bhatti, T. Abbas, M. M. Rashidi, *J. Magn.*, **21**, 468 (2016).
10. M. Khan, A. Shahid, M. Malik, T. Salahuddin, *J. Mol. Liq.*, **251**, 7 (2018).
11. B. J. Gireesha, B. Mahanthesh, G. Thammanna, P. Sampathkumar, *J. Mol. Liq.*, **256**, 139 (2018).
12. S. Gupta, D. Kumar, J. Singh, *Int. J. Heat Mass Transf.*, **118**, 378 (2018).
13. A. Y. Ghaly, *Chaos, Solitons Fract.*, **13**, 1843 (2002).
14. O. D. Makinde, W. A. Khan, Z. H. Khan, *Int. J. Heat Mass Transf.*, **62**, 526 (2013).
15. M. M. Rashidi, M. Nasiri, M. S. Shadloo, Z. Yang, *Heat Transfer Eng.*, **38**, 853 (2017).
16. M. Waqas, M. Farooq, M. I. Khan, A. Alsaedi, T. Hayat, T. Yasmeen, *Int. J. Heat Mass Transf.*, **102**, 766 (2016).
17. G. S. Seth, R. Tripathi, R. Sharma, A. J. Chamkha, *J. Mech.*, **33**, 87 (2017).
18. V. M. Job, S. R. Gunakala, *Int. J. Heat Mass Transf.*, **120**, 970 (2018).
19. M. Mustafa, T. Hayat, I. Pop, S. Asghar, S. Obaidat, *Int. J. Heat Mass Transf.*, **54**, 5588 (2011).
20. K. U. Rehman, A. A. Khan, M. Y. Malik, O. D. Makinde, *J. Braz. Soc. Mech. Sci. Eng.*, **39**, 3669 (2017).
21. M. M. Rashidi, N. Freidoonimehr, *Int. J. Comput. Meth. Eng. Sci. Mech.*, **5**, 345 (2014).
22. G. S. Seth, B. Kumar, R. Nandkeolyar, *J. Nanofluids*, **8**, 620 (2019).
23. I. C. Nelson, D. Banerjee, R. Ponnappan, *J. Thermophys. Heat Tr.*, **23**, 752 (2009).
24. J. Buongiorno, L. W. Hu, S. J. Kim, R. Hannink, B.A.O. Truong, E. Forrest, *Nucl. Technol.*, **162**, 80 (2008).
25. S. M. You, J. H. Kim, K.H. Kim, *Appl. Phys. Lett.*, **83**, 3374 (2003).
26. D. P. Kulkarni, D. K. Das, R. S. Vajjha, *Appl. Energ.*, **86**, 2566 (2009).
27. A. Sharma, V. V. Tyagi, C. R. Chen, D. Buddhi, *Renew. Sust. Energ. Rev.*, **13**, 318 (2009).
28. X. Sun, Z. Liu, K. Welsher, J. T. Robinson, A. Goodwin, S. Zaric, H. Dai, *Nano Res.*, **1**, 203 (2008).
29. T. P. Otanicar, P. E. Phelan, R. S. Prasher, G. Rosengarten, R. A. Taylor, *J. Renew. Sustain. Energ.*, **2**, 033102 (2010).
30. J. Zhou, Z. Wu, Z. Zhang, W. Liu, Q. Xue, *Tribol. Lett.*, **8**, 213 (2000).
31. A. V. Kuznetsov, D. A. Nield, *Int. J. Therm. Sci.*, **77**, 126 (2014).
32. G. K. Batchelor, An Introduction to Fluid Dynamics, Cambridge University Press, Cambridge, 1988.
33. S. W. Yuan, Foundations of fluid mechanics, Prentice Hall,1967.
34. S. S. Motsa, P. Sibanda, *Comput. & Math. with Appl.*, **63**, 1197 (2012).
35. S. S. Motsa, Z. Makukula, *Open Phys.*, **11**, 363 (2013).
36. R. Nandkeolyar, M. Narayana, S. S. Motsa, P. Sibanda, *J. Therm. Sci. Eng. Appl.*, **10,** 061005 (2018).
37. N. Ishfaq, Z. H. Khan, W. A. Khan, R. J. Culham, *J. Hydrodyn. Ser. B*, **28**, 596 (2016).
38. G. S. Seth, R. N. Jana, M. K. Maiti, *Revue Roumaine des Sci. Tech. Ser. de Mécanique Appliquée*, **26**, 383 (1981).
39. S. Sarkar, G. S. Seth, *J. Aerosp. Eng.*, **30,** Article ID 16081 (2016).
40. N. A. Halim, R. U. Haq, N. F. M. Noor, *Meccanica*, **52**, 1527 (2017).

NOMENCLATURE

a, b	arbitrary constants	s	stagnation parameter
B	magnetic field, T	T	fluid temperature, K
C	nanoparticle volume fraction, kg/m^3	T_s	fluid temperature at stretching sheet, K
Cf_x	skin friction coefficient	T_∞	ambient fluid temperature, K
C_∞	ambient species concentration, kg/m^3	u	fluid velocity component in the x direction, ms^{-1}
c_p	specific heat at a constant pressure, $J\,kg^{-1}\,K^{-1}$	u_s	stretching velocity, ms^{-1}
D_B	coefficient of Brownian diffusion	u_∞	free stream fluid velocity, ms^{-1}
D_T	coefficient of thermophoretic diffusion	v	fluid velocity component in the y direction, ms^{-1}
Ec	Eckert number	x, y	coordinate directions, m
f	stream function	α	heat generation parameter
g	gravitational acceleration, ms^{-2}	β	nanofluid volumetric expansion coefficient, K^{-1}
k	thermal conductivity, $Wm^{-1}K^{-1}$	$\theta(\eta)$	dimensionless temperature
Sc	Schmidt number	μ	dynamic viscosity, $kg\,m^{-1}\,s^{-1}$
M	magnetic parameter	υ	kinematic viscosity, m^2s^{-1}
Nb	Brownian motion parameter	ρ_{nf}	nanofluid density, $kg\,m^3$
Nr	buoyancy ratio parameter	$\rho_{nf\infty}$	nanofluid reference density, $kg\,m^3$
Nt	thermophoretic parameter	ρ_{np}	density of nanoparticles, $kg\,m^3$
Nu_x	local Nusselt number	$(\rho c_p)_{nf}$	nanofluid heat capacity
n	constant	$(\rho c_p)_{np}$	nanoparticles heat capacity
Pr	Prandtl number	σ	electric conductivity, $S\,m^{-1}$
Q	heat generation coefficient	λ	mixed convection parameter
q_s	heat flux at the surface, Wm^{-2}	τ_s	surface shear stress $N\,m^{-2}$
Re_x	local Reynolds number	$\phi(\eta)$	dimensionless concentration